Initialization-Wise Quantum Electromagnetic Transient Program

Qi Lou, Yijun Xu, Wei Gu, Fei Zhang
School of Electrical Engineering
Southeast University
Nanjing, Jiangsu 210096, China
{louqi, yijunxu, wgu, zhangfei}@seu.edu.cn

***Abstract*—With the increasing penetration of renewable energy sources and power electronic devices, the Electromagnetic Transients Program (EMTP) has become indispensable for modern power system analysis. Classical EMTP faces a conflict between computational efficiency and real-time requirements, while the rapid advancement of quantum computing offers a pathway for a quantum leap. However, existing QEMTP methods suffer from slow convergence, requiring numerous iterations that consume substantial quantum resources and drastically reduce computational efficiency. This paper proposes an initialization-wise QEMTP framework that leverages physics-informed initialization to accelerate convergence. A detailed analysis of the cost function incorporating the Gram–Schmidt procedure guides the selection of initial parameters, while a cross-initialization method—applied in QEMTP for the first time—mitigates switching-induced errors. Simulation results demonstrate the framework's efficiency, accuracy, and robustness.**

***Index Terms*—Variational quantum linear solver; quantum computing; quantum electromagnetic transients program.**

I. Introduction

With the increasing penetration of power electronic devices and distributed energy resources in modern power systems, the Electromagnetic Transients Program (EMTP) has become an indispensable tool for system planning and operational analysis [1]. However, as the problem scale continues to grow, the $\mathcal{O}(N^3)$ computational complexity of classical EMTP has led to an escalating conflict between computational cost and real-time performance, making classical computing architectures increasingly inadequate to support the high-fidelity, real-time simulation demands of emerging power systems [2].

The rapid development of quantum computing offers a transformative pathway to overcome this computational bottleneck. In 2021, Zhou *et al.* [3] first proposed and validated the concept of the Quantum Electromagnetic Transients Program(QEMTP) based on the HHL algorithm [4]. With the advent of the Noisy Intermediate-Scale Quantum(NISQ) era, research has gradually shifted toward noise-resilient algorithmic designs. Building on the Variational Quantum Linear Solver (VQLS) [5], Zhou *et al.* [6] achieved the first experimental realization of QEMTP on real quantum hardware, extending beyond idealized simulators. In 2025, our previous work further advanced this direction by optimizing the VQLS-based QEMTP through a matrix low-dimensional qubit-casting and real-only construction technique, and subsequently achieving the first implementation for power-electronic-dominated systems based on a quantum fixed-admittance switch model [7].

Nevertheless, existing QEMTP methods still face significant limitations. VQLS-based QEMTP typically require a large number of iterations, which not only consume substantial quantum resources but also drastically reduce computational efficiency—posing a major bottleneck to the practical deployment of QEMTP. To address this issue, we propose an Initialization-wise(Init-wise) QEMTP framework, which leverages physics-informed initialization to achieve a remarkable acceleration in convergence. The main contributions of this paper are as follows:

- A detailed analysis of the VQLS loss function is conducted based on the Gram–Schmidt procedure, and a physics-informed Initialization-wise QEMTP framework is developed to significantly enhance convergence speed.
- The cross-initialization method is introduced into QEMTP for the first time, effectively mitigating switching errors in quantum fixed-admittance switch model for power-electronic-dominated networks.

The simulation results reveal excellent performance of the proposed method.

The remainder of the paper is organized as follows. Section II summarizes the VQLS-Based QEMTP, Section III analyzes the influence of initialization on the convergence incorporating the Gram–Schmidt procedure and presents the proposed Initialization-wise QEMTP framework. Section IV provides case studies, followed by the conclusion in Section V.

II. Preliminary

A. Formulations of the QEMTP

Classical EMTP approach relies on linearization and Norton equivalent principles, approximating complex electrical components as equivalent resistors and current sources for simulation and solution [8]. The matrix form of the EMTP equations is given by

$$\mathbf{G}\vec{v}(t) = \vec{i}_{\text{inj}}(t) + \vec{I}_{\text{his}} \equiv \vec{i}(t). \tag{1}$$

Here, $\mathbf{G}$ denotes the network admittance matrix, $\vec{v}(t)$ denotes the vector of nodal voltages in the network, $\vec{i}(t)$ denotes the vector of nodal injected current vector, $\vec{i}_{\text{inj}}(t)$ denotes the externally injected current in the current time step, and $\vec{I}_{\text{his}}$ denotes the vector of historical nodal injected current.

979-8-3315-8138-1

Once the EMTP equations are formulated, voltages and currents at each time step can be calculated via iterative loops. To extend this framework to quantum computing, the classical EMTP algorithm must be mapped onto the Hilbert space. Rewriting (1) in its quantum form yields[1]:

$$\tilde{\mathbf{G}}|v\rangle = |i\rangle. \tag{2}$$

Here, $\tilde{\mathbf{G}}$ is $\mathbf{G}$ expanded to dimension $2^{\lceil \log_2 N \rceil}$ by padding an identity block in the bottom-right corner and rescaled to have unit determinant. $|v\rangle$ and $|i\rangle$ denote the normalized quantum representations of $\vec{v}(t)$ and $\vec{i}(t)$ respectively, encoded on $n = \lceil \log_2 N \rceil$ qubits:

$$|v\rangle = \frac{\sum_j v_j|j\rangle}{\|\sum_j v_j|j\rangle\|_2}, \quad |i\rangle = \frac{\sum_j i_j|j\rangle}{\|\sum_j i_j|j\rangle\|_2}. \tag{3}$$

Here, v_j and i_j denote the j-th elements of the normalized nodal voltage and current vector respectively.

Based on (2), we next describe how the system can be solved using quantum computing techniques.

B. The Traditional VQLS-Based QEMTP solver

The VQLS algorithm is employed to solve (2) due to its ability to efficiently handle noise and errors in real quantum devices. VQLS represents the solution vector $|v\rangle$ as a parameterized quantum circuit and iteratively optimizes the parameters θ using a classical optimizer. The detailed procedure is as follows.

1) System Parameter Preprocessing: First, to transform (2) into a physically executable quantum circuit, system parameters must be preprocessed. The admittance matrix $\mathbf{G}$ can be decomposed as:

$$\tilde{\mathbf{G}} = \sum_{i=1}^{4^n} c_i \mathbf{g}_i, \quad c_i = \frac{1}{2^n} Tr\left(\tilde{\mathbf{G}} \times \mathbf{g}_i\right). \tag{4}$$

Here, $\mathbf{g}_i \in \otimes_{k=1}^{n}\{I, X, Y, Z\}$, denotes the i-th matrix basis in the set of multi-qubits Pauli gates[2]. c_i denotes the projection coefficient of matrix $\tilde{\mathbf{G}}$.

Then, based on the top-down encoding approach [9], the current state $|i\rangle$ is amplitude-encoded as

$$|i\rangle = \mathbf{U}|0\rangle. \tag{5}$$

Here, $\mathbf{U}$ is a quantum circuit representing a unitary matrix, which enables the nodal injection current $\vec{i}$ to be encoded in the amplitudes of the quantum state.

Meanwhile, the target nodal voltage state $|v\rangle$ is represented as a trainable parameterized quantum circuit, which is the core idea of variational quantum algorithms [10]:

$$|v\rangle = \mathbf{V}(\theta)|0\rangle \tag{6}$$

Here, $\mathbf{V}(\theta)$ denotes a Hardware-Efficient Ansatz composed of a series of rotation gates and multi-qubit entangling gates [11].

[1]In this paper, the Dirac notation $|\cdot\rangle$ is used to represent vectors in the underlying Hilbert space, which are not necessarily normalized unless explicitly stated as 'quantum states'."

[2]The four Pauli gates correspond mathematically to the Pauli operators given as $I = \begin{bmatrix}1 & 0\\ 0 & 1\end{bmatrix}$, $X = \begin{bmatrix}0 & 1\\ 1 & 0\end{bmatrix}$, $Y = \begin{bmatrix}0 & -i\\ i & 0\end{bmatrix}$, $Z = \begin{bmatrix}1 & 0\\ 0 & -1\end{bmatrix}$.

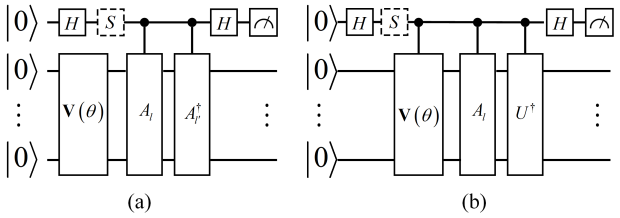

Fig. 1. Quantum circuits based on the Hadamard test for computing C_G: (a) Quantum circuit for evaluating $\beta_{ll'}$; (b) Quantum circuit for evaluating $\gamma_{ll'}$.

2) Cost Function Construction: Next, a cost function is constructed to quantify the similarity between $\tilde{\mathbf{G}}|v\rangle$ and $|i\rangle$. Let $|\psi\rangle \equiv \tilde{\mathbf{G}}|v\rangle$, the global cost function is then defined as:

$$C_G = 1 - \frac{|\langle i|\psi\rangle|^2}{\langle\psi|\psi\rangle} \tag{7}$$

By substituting(4), (6), and (5) into (7), we obtain:

$$\langle\psi|\psi\rangle = \sum_{ll'} c_l c_{l'}^* \beta_{ll'}, \quad |\langle i|\psi\rangle|^2 = \sum_{ll'} c_l c_{l'}^* \gamma_{ll'}, \tag{8a}$$

$$\beta_{ll'} = \langle \mathbf{0}|\mathbf{V}(\theta)^\dagger \tilde{\mathbf{G}}_{l'}^\dagger \tilde{\mathbf{G}}_l \mathbf{V}(\theta)|\mathbf{0}\rangle \tag{8b}$$

$$\gamma_{ll'} = \langle \mathbf{0}|\mathbf{U}^\dagger \tilde{\mathbf{G}}_l \mathbf{V}(\theta)|\mathbf{0}\rangle\langle \mathbf{0}|\mathbf{V}(\theta)^\dagger \tilde{\mathbf{G}}_{l'}^\dagger \mathbf{U}|\mathbf{0}\rangle \tag{8c}$$

Here, $\dagger$ denotes the conjugate transpose. Based on the Hadamard test, quantum circuits can be constructed to evaluate (8b) and (8c), ultimately enabling the computation of (7) [12]. The corresponding circuit structures are illustrated in Fig. 1.

3) Optimal Parameter Training: Now, the VQLS algorithm optimizes the parameters α to be as close to zero as possible. This optimization can be achieved using gradient descent-based methods as

$$\alpha_{k+1} = \alpha_k - \eta \nabla C_L(\alpha). \tag{9}$$

Here, α_k represents the parameters in the k th iteration, η is the learning rate, and $\nabla C_L(\alpha)$ is the cost function gradient with respect to the parameters, α_k . For quantum circuits, the gradient is calculated using the parameter shift rule.

The final node voltage $|\tilde{v}\rangle$ is obtained from the optimized circuit $\mathbf{V}(\theta_{opt})|0\rangle$ and can be iteratively refined using the residual error $\epsilon_i = \left\||i\rangle - \tilde{\mathbf{G}}|\tilde{v}\rangle\right\|_2$ to meet the desired accuracy.

Till now, we have finished the presentation of the VQLS algorithm to solve the QEMTP.

III. The Proposed Init-wise QEMTP

Although the VQLS-base QEMTP theoretically promising, the optimization landscape of $V(\theta)$ is often highly complex, leading to slow convergence [13]. In this section, we introduce an Init-wise QEMTP framework that exploits the physical properties inherent in EMTP to accelerate convergence via informed initialization.

A. Impact of Initial State on Cost Function

First, we examine small perturbations δ around the optimal parameters θ_{opt} in (7). Define $|\hat{v}\rangle = V(\theta_{\text{opt}})|0\rangle$, and let $|\delta v\rangle = (\mathbf{V}(\theta_{\text{opt}}+\delta) - \mathbf{V}(\theta_{\text{opt}}))|0\rangle$, $|\hat{\psi}\rangle = \tilde{\mathbf{G}}|\hat{v}\rangle$ and $|\delta\psi\rangle = \tilde{\mathbf{G}}|\delta v\rangle$. Then, we have:

$$C_G(\theta+\delta) = 1 - \frac{|\langle i|\hat{\psi}+\delta\psi\rangle|^2}{\langle\hat{\psi}+\delta\psi|\hat{\psi}+\delta\psi\rangle}. \tag{10}$$

Expanding (10), and defining $\alpha \equiv |\langle i|\hat{\psi}\rangle|$, $\delta\alpha \equiv |\langle i|\delta\psi\rangle|$, we obtain:

$$C_G(\theta+\delta) = 1 - \frac{\alpha^2 + 2\Re(\alpha^*\cdot\delta\alpha) + \delta\alpha^2}{\langle\hat{\psi}|\hat{\psi}\rangle + 2\Re(\langle\delta\psi|\hat{\psi}\rangle) + \langle\delta\psi|\delta\psi\rangle}. \tag{11}$$

We rewrite (11) as:

$$C_G(\theta+\delta) = 1 - \Psi\frac{1}{1+\eta}, \tag{12a}$$

$$\Psi = \frac{\alpha^2 + 2\Re(\alpha^*\cdot\delta\alpha) + \delta\alpha^2}{\langle\hat{\psi}|\hat{\psi}\rangle}, \tag{12b}$$

$$\eta = \frac{2\Re(\langle\delta\psi|\hat{\psi}\rangle) + \langle\delta\psi|\delta\psi\rangle}{\langle\hat{\psi}|\hat{\psi}\rangle}. \tag{12c}$$

Considering the formulation in (12a), we analyze the regime near the optimal point. In this vicinity, η is primarily governed by the small perturbation $|\delta\psi\rangle$, and can thus be regarded as a small quantity as well. Therefore, we adopt the following approximation:

$$\frac{1}{1+\eta} = 1 - \eta + \eta^2 + \mathcal{O}(\eta^3). \tag{13}$$

By substituting (13) into (12) and neglecting higher-order terms above the second order, we separate the terms up to the second order and obtain:

$$0 \text{ Order:} \quad 1 - \frac{\alpha^2}{\langle\hat{\psi}|\hat{\psi}\rangle} \tag{14a}$$

$$1^{\text{st}} \text{ Order:} \quad 2\frac{\alpha^2\Re(\langle\delta\psi|\hat{\psi}\rangle)}{\langle\hat{\psi}|\hat{\psi}\rangle^2} - 2\frac{\Re(\alpha^*\cdot\delta\alpha)}{\langle\hat{\psi}|\hat{\psi}\rangle} \tag{14b}$$

$$2^{\text{nd}} \text{ Order :} \quad \frac{\alpha^2\langle\delta\psi|\delta\psi\rangle}{\langle\hat{\psi}|\hat{\psi}\rangle^2} - \frac{\delta\alpha^2}{\langle\hat{\psi}|\hat{\psi}\rangle} - \frac{\alpha^2}{\langle\hat{\psi}|\hat{\psi}\rangle}\frac{4\Re(\langle\delta\psi|\hat{\psi}\rangle)^2}{\langle\hat{\psi}|\hat{\psi}\rangle^2} + \frac{4\Re(\alpha^*\cdot\delta\alpha)\Re(\langle\delta\psi|\hat{\psi}\rangle)}{\langle\hat{\psi}|\hat{\psi}\rangle^2}. \tag{14c}$$

Since (7) essentially computes the projection of $|\hat{\psi}\rangle$ onto $|i\rangle$, the two vectors become collinear at the optimal point. We assume $|\hat{\psi}\rangle = \gamma|i\rangle$. Given that $|i\rangle$ is normalized, the following properties hold:

$$\alpha^2 = (\gamma\langle i|i\rangle)^2 = \gamma^2 = \langle\hat{\psi}|\hat{\psi}\rangle, \tag{15a}$$

$$\Re(\langle\delta\psi|\hat{\psi}\rangle) = \gamma\Re(\langle\delta\psi|i\rangle) = \Re(\alpha^*\cdot\delta\alpha). \tag{15b}$$

Substituting (15) into (14), one can observe that **the zero-order term, first-order term, and the cross terms in the second-order term of (14) are all eliminated.** The resulting form is:

$$C_G(\theta+\delta) = \frac{\langle\delta\psi|\delta\psi\rangle - \delta\alpha^2}{\langle\hat{\psi}|\hat{\psi}\rangle} + \mathcal{O}(\eta^3). \tag{16}$$

Further considering (16), we first orthogonally decompose $|\delta\psi\rangle$ along $|\hat{\psi}\rangle$ using the Gram–Schmidt procedure [14], yielding:

$$|\delta\psi\rangle = \frac{\langle\hat{\psi}|\delta\psi\rangle}{\langle\hat{\psi}|\hat{\psi}\rangle}|\hat{\psi}\rangle + P_\perp^{|\psi\rangle}(|\delta\psi\rangle), \quad P_\perp^{|\psi\rangle} = I - \frac{|\psi\rangle\langle\psi|}{\||\psi\rangle\|_2^2}. \tag{17}$$

Here, $|\delta\psi_\perp\rangle$ Here, $P_\perp^{|\psi\rangle}$ denotes the projection operator that projects $|\delta\psi\rangle$ onto the subspace orthogonal to $|\hat{\psi}\rangle$. Substituting (17) into the definition of $\delta\alpha$ yields:

$$\delta\alpha \equiv |\langle i|\delta\psi\rangle| = \frac{|\langle\hat{\psi}|\delta\psi\rangle|}{\left\||\hat{\psi}\rangle\right\|_2}. \tag{18}$$

Substituting (17) and (18) into (16) yields the final expression:

$$C_G(\theta+\delta) = \frac{\left\|P_\perp^{|\psi\rangle}(\tilde{\mathbf{G}}|\delta v\rangle)\right\|_2^2}{\left\|\tilde{\mathbf{G}}|\hat{v}\rangle\right\|_2^2} + \mathcal{O}(\eta^3). \tag{19}$$

Since projection does not increase the norm, we can derive the following inequality based on the norm definition:

$$\left\|P_\perp^{|\psi\rangle}(\tilde{\mathbf{G}}|\delta v\rangle)\right\|_2^2 \le \left\|\tilde{\mathbf{G}}|\delta v\rangle\right\|_2^2 \le \left\|\tilde{\mathbf{G}}\right\|_2^2 \||\delta v\rangle\|_2^2. \tag{20}$$

From (20), the upper bound of (19) can be derived as follows:

$$C_G(\theta+\delta) \le c_{\max}\||\delta v\rangle\|_2^2, \quad c_{\max} = \frac{\left\|\tilde{\mathbf{G}}\right\|_2^2}{\left\|\tilde{\mathbf{G}}|\hat{v}\rangle\right\|_2^2}. \tag{21}$$

Based on the singular value decomposition, the upper bound of $c_{\max}$ in (21) is the squared condition number $\kappa(\tilde{\mathbf{G}})^2$, yielding the final upper-bound estimation:

$$C_G(\theta+\delta) \le \kappa(\tilde{\mathbf{G}})^2\||\delta v\rangle\|_2^2. \tag{22}$$

Remark 1. *The relationship expressed in (22)—a quadratic sensitivity of the cost function to the state deviation $|\delta v\rangle$ near its optimum—is the central finding of this section. This elegant upper bound is the culmination of our derivation, which originally employed the Gram–Schmidt procedure to dissect the cost function's geometry. The practical implication of this quadratic behavior is profound: it validates the strategy of prioritizing a high-quality initial point, which dramatically accelerates convergence. Thus, our theoretical analysis provides the essential justification for the proposed Init-wise QEMTP framework.*

B. Physics-informed Initialization Choice

Building upon the previous analysis, it becomes evident that the choice of the initial point critically influences the convergence behavior of the VQLS-based QEMTP. In this section, we further explore how this insight can be practically utilized in time-domain simulations.

Let $|v_{(t)}\rangle$ and $|i_{(t)}\rangle$ denote the quantum states of node voltage and current at time step t, respectively. Based on (2), we have:

$$|v_{(t)}\rangle = \tilde{\mathbf{G}}^{-1}|i_{(t)}\rangle. \tag{23}$$

Define $|\Delta i_{(t)}\rangle$ as the difference between the current quantum states at time step $t+\Delta t$ and t, and let $|v_{t+\Delta t}\rangle$ denote the voltage quantum state at the next time step. Then, we have:

$$|v_{t+\Delta t}\rangle = |v_{(t)}\rangle + \tilde{\mathbf{G}}^{-1}|\Delta i_{(t)}\rangle. \tag{24}$$

Let $|v_t^{\text{ans}}\rangle$ denote the QEMTP solution obtained at time step t. The corresponding solution error ϵ_{prev} is defined as:

$$\epsilon_{\text{prev}} = \left\| |v_{(t)}\rangle - |v_{(t)}^{\text{ans}}\rangle \right\|_2. \tag{25}$$

We define the error between $|v_{(t+\Delta t)}\rangle$ and $|v_{(t)}^{\text{ans}}\rangle$ as ϵ_t. Combining (24) and (25), we obtain:

$$\begin{aligned} \epsilon_t &= \left\| |v_{(t+\Delta t)}\rangle - |v_{(t)}^{\text{ans}}\rangle \right\|_2 \\ &\le \epsilon_{\text{prev}} + \left\| \tilde{\mathbf{G}}^{-1} \right\|_2 \left\| |\Delta i_{(t)}\rangle \right\|_2 \end{aligned} \tag{26}$$

For $|\Delta i_{(t)}\rangle$, since the time step Δt in EMTP simulations is typically small ($\le 10^{-3}$), it can be approximated using the first-order time derivative of the current state $|\dot{i}_{(t)}\rangle$:

$$|\Delta i_{(t)}\rangle = |\dot{i}_{(t)}\rangle \Delta t + \mathcal{O}(\Delta t^2) \tag{27}$$

Omitting the second-order terms and substituting (27) into (26), we obtain:

$$\epsilon_t \le \epsilon_{\text{prev}} + \frac{\kappa(\tilde{\mathbf{G}})}{\left\| \tilde{\mathbf{G}} \right\|_2} \left\| |\dot{i}_{(t)}\rangle \right\|_2 \Delta t \tag{28}$$

(28) justifies our choice of initial point. During continuous operation, since $|\dot{i}_{(t)}\rangle$ is bounded, ϵ_t remains a first-order small quantity. Hence, the previous solution serves as an excellent initial guess that keeps the initial error low and accelerates convergence.

For discontinuities such as switching or faults, the pre- and post-disturbance states can still be viewed as two adjacent steady conditions. At the instant of change, $|\delta i\rangle$ can no longer be approximated by (27). Nevertheless, $|v_t^{\text{ans}}\rangle$ remains an effective approximation, yielding a superior initialization compared to random schemes, as will be demonstrated in Section IV.

C. Initialization-wise QEMTP Framework

Accordingly, we propose an Initialization-wise (Init-wise) QEMTP framework, as illustrated in Algorithm 1. At the initial time step, the variational parameters $\theta_{(0)}^0$ are randomly initialized. For subsequent steps, a warm-start strategy is adopted, where the optimized parameters from the previous step, $\theta_{(t-1)}^{opt}$, are reused as the initial parameters $\theta_{(t)}^0$. This approach not only accelerates the convergence of VQLS but also provides a physically meaningful initialization by leveraging the system's historical state information.

In power-electronic-dominated networks, the conventional quantum fixed-admittance switch model in QEMTP often causes pronounced state discontinuities at switching instants. These discontinuities degrade simulation accuracy and make the previous system state unsuitable as an effective initial point. To address this issue, a cross-initialization method [15]—applied for the first time in QEMTP—is introduced for such networks. By exchanging the historical current terms of switches within the same bridge arm before the $|i\rangle$ encoding during topology transitions, this method effectively suppresses the initial-value errors induced by state switching. Consequently, it not only enhances the simulation accuracy of systems with dynamic topologies but also mitigates transient error fluctuations, ensuring that the proposed framework maintains robust convergence acceleration even under frequent switching operations.

Algorithm 1 Initialization-wise Quantum Electromagnetic Transient Program (Init-wise QEMTP)

Require: T_{end}, ϵ_{set} and system parameters
Construct admittance matrix $\mathbf{G}$ and encode as $\tilde{\mathbf{G}}$
Encode $\mathbf{G}$ into quantum circuit representation using (4)
for $t = 0$ to T **do**
  Compute $\vec{I}_{\text{his}}(t)$ for each component
  ▷ *Cross-initialization Method*
  if Switching event occurs **then**
    Identify the paired switches i and j
    Exchange $\vec{I}_{\text{his}}(t)[i]$ and $\vec{I}_{\text{his}}(t)[j]$
  end if
  Construct $\vec{i}(t)$ via (1) and prepare $|i_{(t)}\rangle$ using (3).
  Encode $|i_{(t)}\rangle$ into quantum circuit via (5).
  ▷ *Warm-start strategy*
  if $t = 0$ **then**
    $\theta_{(0)}^0 \leftarrow$ random initialization
  else
    $\theta_{(t)}^0 \leftarrow \theta_{(t-1)}^{opt}$
  end if
  Obtain $\theta_{(t)}^{opt}$ and $|v_{(t)}^{ans}\rangle$ using VQLS with tolerance ϵ.
  Rescale $|v_{(t)}^{ans}\rangle$ to obtain $\vec{v}(t)$ via (3)
  Update output voltage array: $v_{\text{output}} \leftarrow \{v_{\text{output}}, \vec{v}(t)\}$
end for
▷ *Output:* Time-series QEMTP results v_{output}

IV. Case Studies

The effectiveness of the proposed method is validated on a three-phase full-bridge converter, whose topology is illustrated in Fig. 2(a). The system is driven by an ideal three-phase AC source with an RMS line voltage of 400 V. The rectifier is equipped with a DC-link capacitor of 4 mF, an inductance of 0.5 mH, and a resistive load of 100 Ω, which is abruptly reduced to 50 Ω at 0.02s to emulate a sudden load increase. The SPWM modulation frequency is set to 2.5 kHz. To comprehensively assess the model's accuracy, open-loop simulations are conducted with a time step of 10 μs. The QEMTP accuracy threshold ϵ_{set} is set to 10^{-10}, and the ansatz depth is configured to five layers.

We compare the classical EMTP with binary resistance modeling, the traditional QEMTP, and the proposed Init-wise QEMTP. The results are shown in Fig. 2. As observed from Figs. 2(b) and (c), the cross-initialization method effectively

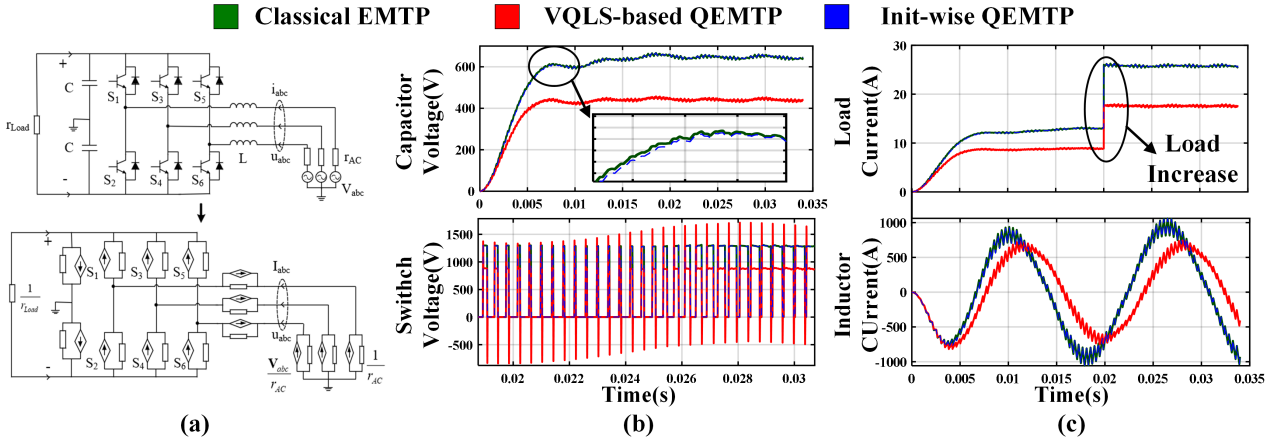

Fig. 2. Topology and simulation results of the three-phase converter: (a) topology of the three-phase full-bridge converter; (b) voltage waveforms; and (c) current waveforms.

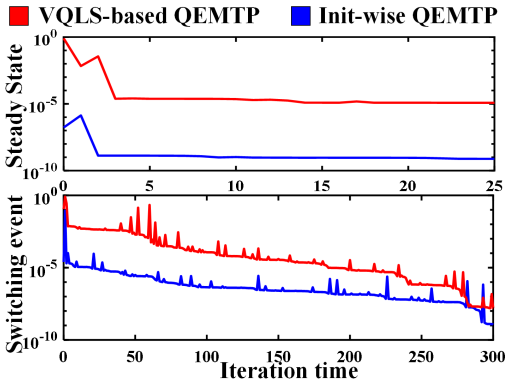

Fig. 3. VQLS iteration performance

suppresses simulation errors during switching instants, thereby significantly improving the overall waveform accuracy.

As illustrated in Fig. 3, under steady-state conditions, the Init-wise QEMTP achieves a substantial reduction in the number of iterations required for convergence—only 25 iterations are needed to reach the predefined threshold, compared with 462 iterations in the conventional approach, representing more than an 18-fold improvement. Even during switching events, the proposed framework also achieves a noticeable reduction in iteration count. On average, the VQLS-based QEMTP requires 364 iterations to converge, whereas the Init-wise QEMTP achieves convergence in only 103 iterations, yielding over a threefold acceleration.

In this case study, each iteration involves 1,860 quantum circuit evaluations; thus, during a 0.034-second simulation, the Init-wise QEMTP saves more than **1.6 billion** quantum circuit executions—a remarkable reduction in quantum computational cost. Throughout the simulation, both quantum approaches maintain errors below 10^{-10}, satisfying the predefined accuracy criterion.

V. Conclusion

This paper proposes an initialization-wise QEMTP framework, validated for power-electronic-dominated systems through the incorporation of a cross-initialization method. Simulation results show that the proposed framework significantly accelerates convergence and consequently reduces quantum resource consumption while maintaining high accuracy, thereby advancing the practical realization of QEMTP.

References

[1] N. Watson, J. Arrillaga, and J. Arrillaga, *Power systems electromagnetic transients simulation*. Iet, 2003, vol. 39.

[2] S. Golestan, M. Habibi, S. Mousazadeh Mousavi, J. Guerrero, and J. Vasquez, "Quantum computation in power systems: An overview of recent advances," *Energy Reports*, vol. 9, pp. 584–596, 2023.

[3] Y. Zhou, F. Feng, and P. Zhang, "Quantum electromagnetic transients program," *IEEE Transactions on Power Systems*, vol. 36, no. 4, pp. 3813–3816, 2021.

[4] A. W. Harrow, A. Hassidim, and S. Lloyd, "Quantum algorithm for linear systems of equations," *Physical review letters*, vol. 103, no. 15, p. 150502, 2009.

[5] C. Bravo-Prieto *et al.*, "Variational quantum linear solver," *Quantum*, vol. 7, p. 1188, 2023.

[6] Y. Zhou, P. Zhang, and F. Feng, "Noisy-intermediate-scale quantum electromagnetic transients program," *IEEE Transactions on Power Systems*, vol. 38, no. 2, pp. 1558–1571, 2022.

[7] Q. Lou, Y. Xu, and W. Gu, "Matrix low-dimensional qubit casting based quantum electromagnetic transient network simulation program," *arXiv preprint arXiv:2502.11728*, 2025.

[8] H. Dommel, *EMTP Theory Book*. Microtran Power System Analysis Corporation,Vancouver, Canada, 1992.

[9] I. F. Araujo *et al.*, "Configurable sublinear circuits for quantum state preparation," *Quantum Information Processing*, vol. 22, no. 2, Feb. 2023. [Online]. Available: http://dx.doi.org/10.1007/s11128-023-03869-7

[10] M. Cerezo *et al.*, "Variational quantum algorithms," *Nature Reviews Physics*, vol. 3, no. 9, pp. 625–644, 2021.

[11] A. Kandala *et al.*, "Hardware-efficient variational quantum eigensolver for small molecules and quantum magnets," *nature*, vol. 549, no. 7671, pp. 242–246, 2017.

[12] D. Aharonov, V. Jones, and Z. Landau, "A polynomial quantum algorithm for approximating the jones polynomial," in *Proceedings of the thirty-eighth annual ACM symposium on Theory of computing*, 2006, pp. 427–436.

[13] M. Cerezo, A. Sone, T. Volkoff, L. Cincio, and P. J. Coles, "Cost function dependent barren plateaus in shallow parametrized quantum circuits," *Nature communications*, vol. 12, no. 1, p. 1791, 2021.

[14] Å. Björck, "Numerics of gram-schmidt orthogonalization," *Linear Algebra and Its Applications*, vol. 197, pp. 297–316, 1994.

[15] Y. Cao *et al.*, "A bridge-arm-module-based fixed-admittance adc model for converters in emt simulation," *IEEE Transactions on Power Delivery*, 2025.